Pro Gradu

Thin film conductivity measurements of carbon nanotube hemicellulose complex

Ville Saunajoki

5th of December 2014

UNIVERSITY OF JYVÄSKYLÄ
DEPARTMENT OF PHYSICS
NANOSCIENCE CENTER

Preface

Reported work has been done between June 2013 and December 2014 at Nanoscience Center, Department of Physics in University of Jyväskylä.

First I would like to thank my supervisor Prof. Markus Ahlskog for interesting projects and guidance during the time I have worked in the Molecular Technology group. I thank also Jorma Virtanen and Veijo Kangas of nEMCel Ltd. for providing this project with novel material.

I want to thank also Dr. Peerapong Yotprayoonsak for the help with many practicalities considering the measurements and for many interesting discussions. I want to thank also the other members of our group and the Nanoscience Center staff too.

Ville Saunajoki
December 2014

Tiivistelmä

Työssä mitattiin hiilinanoputkista ja hemiselluloosasta koostuvan läpinäkyvän ohutkalvon sähkönjohtavuutta. Materiaali on Nemcel Oy:n kehittämä. Valmistimme useita näytteitä erilaisia mittauksia varten ja testataksemme eri valmistusmenetelmiä.

Valmistetun ohutkalvon merkittävimmät ominaisuudet ovat läpinäkyvyys ja hyvä sähkönjohtavuus. Valmistetut kalvot olivat pääasiassa läpinäkyviä, mikä edellytti kalvon ohuutta. Itse materiaali toimitettiin vesiliuoksena, jossa oli 1:1 hiilinanoputkia ja hemiselluloosaa. Kalvot valmistettiin joko spinnaamalla tai kuivattamalla yksittäisiä pisaroita pinnalle. Näytteet valmistettiin pintaoksidioidulle piille, johon oli tehty kultaelektrodit.

Kalvoa kuvattiin optisella-, atomivoima- ja elektronitransmissio mikroskoopeilla. Optinen kuvantaminen osoitti kalvon epätasaisuuden. Atomivoimamikroskoopilla saatiin kuva kalvon kuitumaisesta hienorakenteesta, sekä pystyttiin määrittämään kalvon paksuus. Rakenteessa havaittiin hiilinanoputkista muodostuvia renkaita, joita päätettiin kuvata tarkemmin elektronitransmissiomikroskoopilla. Näissä kuvissa nähtiin renkaiden käämiä muistuttava rakenne.

Sähkönjohtavuusmittauksia tehtiin useita ja niissä käytettiin nelipistemittausta. Ensimmäisenä mitattiin luonnollisesti johtavuus huoneilmassa, mistä siirryttiin matalan lämpötilan mittauksiin. Näytteet jäähdytettiin noin 4,2 K:iin, minkä aikana niiden johtavuuden havaittiin heikkenevän ensin hyvin hitaasti ja lopuksi, kymmenien kelvinien lämpötilassa, nopeammin. Matalassa lämpötilassa virran ja jännitteen suhteen havaittiin muuttuvan epälineaariseksi. Transistoriominaisuuksia testattiin myös 4,2 K:ssa, mutta niitä ei havaittu. Jäähdytyksen aikana kerätyn datan havaittiin noudattavan pääasiassa VRH-mallia (variable range hopping), joka on eräs tapa kuvata sähkönjohtavuuden lämpötilariippuvuutta epäsäännöllisen hilan materiaaleissa.

Kalvon sähkönjohtokykyä testattiin myös muissa olosuhteissa. Ilman kosteuden huomattiin heikentävän kalvon johtavuutta selkeästi noin 50 % :n suhteellisen kosteuden yläpuolella ja johtavuus palautui ennalleen erittäin hitaasti. Johtavuutta yritettiin mitata myös kalvoa lämmitettäessä huoneil-

maa korkeampiin lämpötiloihin, mutta karkeasti toteutetulla laitteistolla ei onnistuttu saamaan luotettavia tuloksia lämmityksen vaikutuksesta.

Contents

1 Introduction

Carbon nanotube (CNT) thin films have been developed in recent years for transparent conductors.[1–3] They could have several applications in opto-electronics where indium tin oxide (ITO) is mainly used. The main worry with ITO is that indium resources are running out. In addition deposition processes of ITO are expensive and the final product is very sensitive to bending. By doping CNT films can achieve high conductivities to compete with ITO[4] but also other applications exist such as electromagnetic shielding.[5]

Usually CNT film fabrication requires the dispersing of CNT to some solvent. The safest and cheapest possible solvent is water but CNTs do not disperse to water on their own and require some sort of dispersant. Different polysaccharides have shown to be possible dispersants for CNT.[6–8] In this work hemicellulose, xylan, has been used for dispersion of double-walled CNTs (DWCNT). Film is made out of the solution and the cellulose is left to the final film unlike in many other methods where the dispersants are rinsed from the final film.

2 Theory

2.1 Electrical conductivity

Material's intrinsic ability to conduct electricity can be described by electrical conductivity. An other widely used measure is the resistivity which is the reciprocal of conductivity. These intrinsic quantities are good for material comparison but often they are derived from resistance of certain sized piece of material.

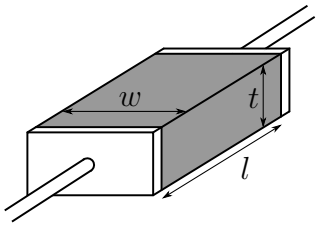

Figure 1: Piece of material in electric measurement and its dimensions.

If resistance R is measured for object such as in figure 1, its electric volume conductivity σ is defined as

$$\sigma = \frac{1}{\rho} = \frac{l}{Rwt}, \tag{1}$$

where l, w and t are dimensions – ρ is the resistivity. The unit of volume conductivity is S/m which might get easily confused with one dimensional conductivity. In this theses, when conductivity is mentioned in general, it refers to electric volume conductivity of a material.

With thin films also surface resistivity (or sheet resistance) is used for material comparison. This quantity is thickness independent and can be preferred for example in cases where equal thickness's of different materials is used and the situation can be considered as two dimensional. For surface resistivity R_s applies

$$R_s = \frac{Rw}{l}, \tag{2}$$

where R is again the resistance and w and l are the dimensions shown in

figure 1. The units of dimension cancel each others out in the equation and for the unit is left Ω. To tell the difference to bulk resistance, Ω/sq or Ω/□ are used instead.

2.2 Four point measurement

Four point measurement is used in accurate resistance measurements. In-line version of measurement circuit is shown in figure 2. When the current travels from current source through the circuit, voltage losses occur along wires, electrodes and film but also at contacts between them. Contact resistances can compromise the accuracy of voltage measurement if current passes through the voltmeter or if there is unnecessary contacts between the meter and the measured points.

Let's consider the side B of figure 2. The film and voltmeter can be thought as parallel connection. Voltmeters have high internal resistance and that is now significantly higher than the resistance of the film's middle section. It is safe to approximate the current to pass only along the film. The potential on a middle electrode is the same as the voltage on the film section covering it because there is no current through their interface. This ables accurate measurement of voltage difference between the middle electrodes. For comparison, if the voltmeter was connected to outer electrodes, the contact resistance between electrode and film would be included to voltage readings

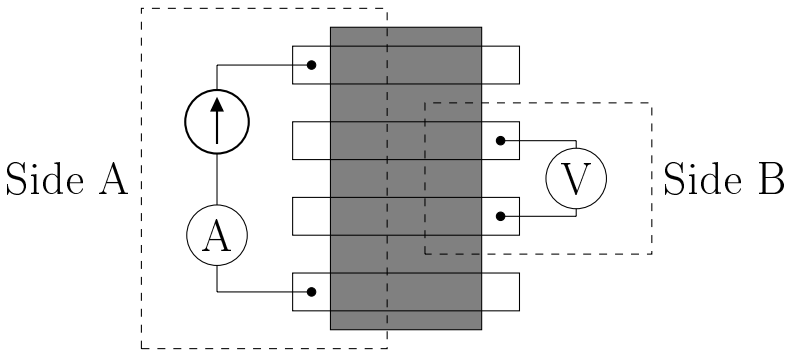

Figure 2: In-line four point measurement circuit used in measurements. The measured film (grey) is cast on four metal electrodes which are the contacts to other parts of setup.

as current would pass trough that interface.

The whole circuit can now be considered as serial connection corresponding to side A. Due to the middle electrodes, accurate voltage difference can be read along a film section between the middle electrodes. As the current has no losses in the circuit, it is constant all along the serial connected circuit.

For derivation of conductivity, the dimensions of the film have to be known. Length of film is closest edge to edge distance between the middle electrodes. The film width is also from the middle section at the point where it is on its narrowest. The equation 1 expects constant thickness so it is taken as average of several thickness readings.

2.3 Carbon nanotube

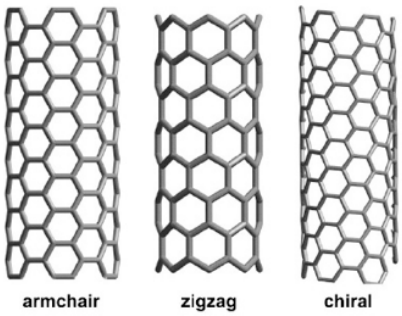

Figure 3: CNTs with different chiralities. (Reprinted [9])

Carbon nanotube (CNT) is an allotrope of carbon where carbon atoms arrange to two dimensional lattice which rolls up as a tube. CNTs can be considered as 1D material as the diameter of the tube can be ~1 nm but the length can be tens of micrometers meaning aspect ratio in several orders of magnitude. The atoms connect to each others with sp^2 bonds forming a hexagonal pattern as in graphene. Closer observation of lattices in different tubes shows variation as it comes to rolling up the pattern which is shown in figure 3.

The lattice of CNT can be described with chirality vector $\vec{C_h}$. Base vectors $\vec{a_1}$ and $\vec{a_2}$ of CNT are shown on graphene lattice in figure 4 and they denote

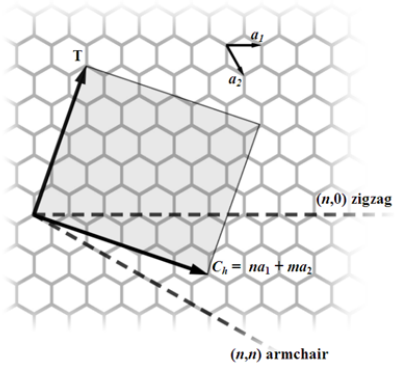

Figure 4: Base vectors $\vec{a_1}$ and $\vec{a_2}$ shown on graphene lattice.*Base vectors are used to define the chirality vector $\vec{C_h}$ and the perpendicular translation vector $\vec{T}$. (Reprinted [12])

the chirality vector

$$\vec{C_h} = n\vec{a_1} + m\vec{a_2} \qquad \text{,where } n,m \in \mathbb{N}.$$

The integers n and m are used to descibe the tube as (n,m). On tube the chirality vector points the circumference – ends in the same lattice point as where it begins. Other vector which is sometimes used is the translation vector $\vec{T}$ which is perpendicular to $\vec{C_h}$. On tube $\vec{T}$ is parallel to the axis of tube and goes from lattice point to next similar point. Length of the vector $\vec{T}$ gives the unit cell length of a tube.

Different lattice means different electron transport. Depending on the lattice, CNT can be metallic or semiconducting with either narrow or moderate band gap.[10] In the end roughly two thirds of the CNTs are semiconducting.[11]

CNTs may also have several layers of walls. Tubes with one layer are called single walled CNTs (SWCNT) and others can be called multi-walled CNTs (MWCNT) although names as 'double-walled CNT' are used (DWCNT). Structure of MWCNT is shown in figure 5. The MWCNTs have layers with different chiralities and the properties of a whole tube are outcome of different layers. For example DWCNTs can be metallic or semiconducting.

*The selection of base vectors may vary between publications. Selection of base vectors should be checked before comparing calculations.

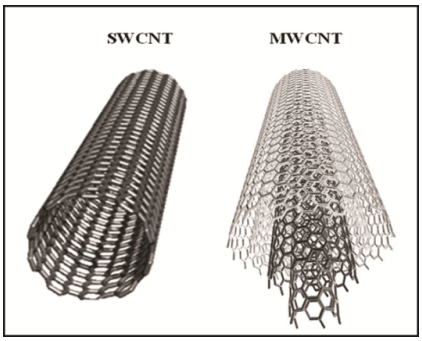

Figure 5: Structural comparison of SWCNT and MWCNT. (Reprinted [13])

2.4 Hemicellulose

Hemicellulose is a polysaccharide which can be found in cell walls of plant cells. Its role is to strengthen the cell walls by binding to cellulose. Compared to normal cellulose hemicellulose polymers are shorter, branched and consist of many different kinds of sugar molecules. Xylan is one of the several types of cellulose and it contains mainly β-D-xylose units. Xylan is the hemicellulose type used in this work.

2.5 Theoretical models of charge transfer in CNT network

Individual carbon nanotube's conductivity depends on its chirality. In practise also electrode contacts and environment play significant role. With CNT networks the situation complicates even more as there are tubes with various chiralities, lengths, contacts and so on.

There are two widely used models to describe network's conductivity as function of temperature: variable range hopping (VRH) and fluctuation-induced tunneling (FIT). Models take a bit different approaches to charge transport and which model applies the best, depends on networks structure. Due to several transport mechanisms in network, the models succeed to describe the behaviour only on range where their approach is the dominant mechanism.

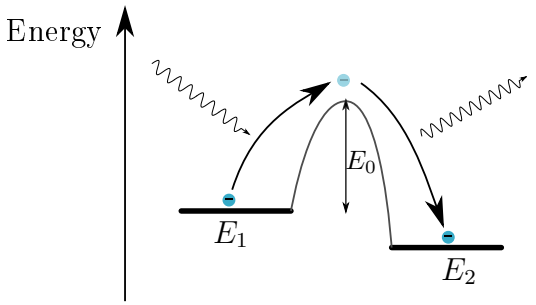

Figure 6: Charge transfer of VRH model. Localized energy states E_1 and E_2 are separated by energy barrier of height E_0. With external energy the electron can hop/clime over the barrier.

2.5.1 Variable range hopping

Mott developed model for amorphous semiconductors, which have localized energy states, to describe its conductivity.[14] The model considers transfer as phonon-assisted hopping.

Let's consider two localized energy states E_1 and E_2 for an electron. Energies of states can differ and the states relate to different lattice points. The states are also separated by an energy barrier (fig. 6). In VRH the transfer is phonon-assisted meaning the electrons gets energy from phonon to overcome the barrier separating the states.

With this approach conductivity's temperature dependency, $\sigma(T)$, has been defined as

$$\sigma = \sigma_0 \exp\left(-T_0/T\right)^{1/(d+1)}, \tag{3}$$

where σ_0 is the conductivity to which the system saturates at high temperature, T_0 is related to activation energy (E_0 of fig. 6) and the d is for dimensionality. Films can be approximated as two dimensional material, $d = 2$, which gives exponent of $1/3$.

2.5.2 Fluctuation induced tunnelling

In 1980 Ping Sheng introduce his model to describe the conductivity of materials consisting of long conducting pathways.[15] The model builds on principle that the conducting parts are separated from each others by energy

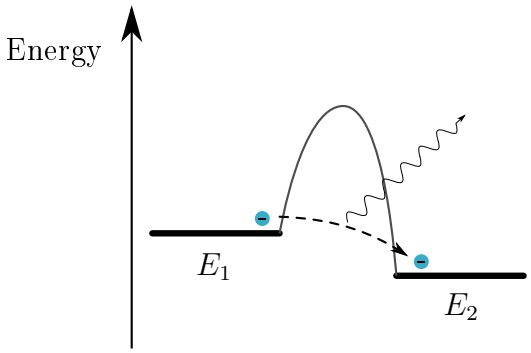

Figure 7: FIT model considers low temperature charge transfer to be dominated by tunnelling through the barrier. After some temperature also charge hopping becomes possible and at high temperatures the hopping is the dominant mechanism.

barriers through which the current can tunnel at lower temperatures.

The model considers two charge transfer mechanisms which dominate at different temperature regions. Let's consider again two different localized energy states E_1 and E_2 which are separated by an energy barrier (fig 7). At low temperatures charge hopping can not occur as the phonon energies are insufficient to raise the electron over the barrier. Anyhow there can be charge transfer between the states in form of tunnelling trough the barrier. Because tunnelling is short range transport the barrier is expected to be narrow.

When the system heats up, the phonon energies rise and at some point charge hopping becomes possible too. For conductivity's relation to temperature has been derived

$$\sigma(T) = \sigma_0 \exp\left(-\frac{T_1}{T_0 + T}\right), \tag{4}$$

where σ_0 is conductivity in room temperature. The temperatures T_1 and T_0 are related to different charge transfer mechanisms. T_1 is the temperature below which tunnelling is the dominant mechanism and T_0 is temperature above which phonon-assisted transfer over the barrier starts to occur. For these two temperatures applies $T_0 < T_1$ as the hopping can occur although the tunnelling is the dominant mechanism.

3 Measurement setups

Our material was know to be conducting. In addition of preparing different samples and measuring their conductivities, the effect of environment was examined. We used couple of setups to control the environment around the measured sample and they are represented more closely in this section.

3.1 Low temperature setup

We used liquid helium dewar based setup for low temperature measurements. The setup schematics is shown in figure 8. Dip-stick is used to sink the sample in liquid helium. Sample is attached to the end of dip-stick and closed inside a chamber. Through the rod of dip-stick goes cables for electric contacts to sample and also gas line to control the chamber conditions.

When temperature drops enough, room air will solidify so it is pumped out of the chamber. When the pressure inside the chamber drops below 10^{-2} mbar the dip-stick is brought close to the dewar. Some helium is let inside the chamber to ensure the heat exchange between the sample and the chamber walls. The dip-stick is slowly lowered to the dewar. Clear boiling sound can be heard from the dewar when the chamber touches the liquid level. The chamber is sunk a bit in the liquid helium and the system is

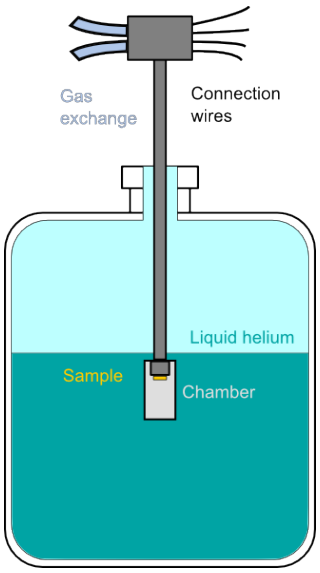

Figure 8: Schematics image of low temperature measurement setup of liquid helium dewar and dip-stick.

left to stabilize. As the temperature difference is hundreds of degrees the thermal expansion is significant. The system is given time to stabilize slowly to prevent any damage.

The boiling point of helium in 1 atm pressure is about 4.2 K and it is the lowest theoretically reachable temperature with this setup. Inside the chamber, right next to the sample, is a DT-450 silicon diode sensor to measure the temperature. The cooling of the chamber slows down as the boiling point of helium is approached. This can be noticed also as fading of the boiling sound. To reach the lowest possible temperature faster the chamber is lowered even more so that it sinks completely under the liquid helium level. Total process of cooling down to ~5 K takes almost one hour.

3.2 Humidity chamber

Self-build setup was used to control the humidity in surroundings of a sample. The setup is shown in figure 9. Sample was attached to measurement box for electric contacts and closed inside plexi glass chamber. Chamber had two connections on walls for gas exchange and hole in ceiling for a humidity sensor. Blu-Tack was used to seal the chamber clearances (contacts to box and ceiling hole).

Steam from boiling water was used as humidity source. Steam was induced to chamber through silicone tubes. Water was boiled on heat plate and directed to silicone tube with a cone. To create flow through the chamber, a fan (CPU cooler) was added in front of the cone. The flow could be controlled by adjusting the voltage of the fan or with a valve added to the gas in-line.

For lower humidities nitrogen gas was used instead. Nitrogen pistol's barrel was fitted in the cone and the clearance was again sealed with blu-tack. The trigger of pistol was bound to fully open position and the flow was controlled with valves of gas lines in addition to the setup's valve.

Before taking each measurement point the humidity was kept constant for a few minutes. Four point measurement was used to define the resistances. Obtaining stable humidity conditions turned out to be difficult with home-

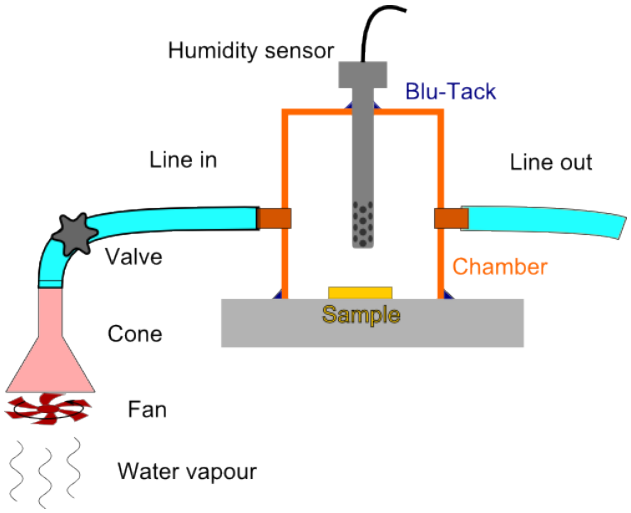

Figure 9: Schematics image of the setup to control the humidity around the sample.

made setup. The resistance measurement took only about a minute but adjusting the conditions for one measurement point could take 30 minutes.

3.3 Heating experiments

We used heat gun to warm the sample to above room temperatures. The sample was attached to measurement box for electrode contacts. To somehow direct and collect the warm air flow, a table light shader was used around the sample. Pt100 thermocouple was installed next to the sample to measure the temperature.

At the beginning of each heating readings were gathered in room temperature to ensure the stability of setup. We wanted to heat the sample slowly so the gun was set to blow further away at first. Once the sample started to heat up, the heat gun was brought closer. Upper limit of heating was set by the soldering tin used in electric contacts. Once the temperature had reached about 150 °C it was kept constant for a while.

Heating to maximum temperature took about a minute. The sample was cooled down by first bringing the heat gun further away from the sample and finally turning it off. The sample was then left to cool down. The sample

was all the time in room air without any chamber.

4 Sample fabrication

In beginning of the project the films were made on clean glass. The first tests were simple two wire resistance measurements with banana connectors as probes. On glass the transparency of the CNT-cellulose film was easy to see. Soon electrodes were made on glass for better electric contacts to the film. As we moved on to low temperature samples the substrate was changed to oxidized silicon. Oxidized surface had the needed insulating property and silicon underneath enabled back gate sweeps.

All conductivity measurements of this report are made with silicon substrate samples. The structure is shown in figure 10.

4.1 Chip structure

Silicon chips were square shaped and about 6 mm on a side. On top they had oxide layer of 300-500 nanometers. First they were cleaned in acetone using cotton sticks and sonication. After washing they were rinsed in isopropanol and dried with nitrogen gun.Four electrodes were evaporated on chips using 3 nm titanium sticking layer and 12 nm gold layer. Layers of structure are shown in figure 10b.

The patterning of electrodes was carried out by painting PMMA with cotton stick to the edges of a chip and then using a mask during metal

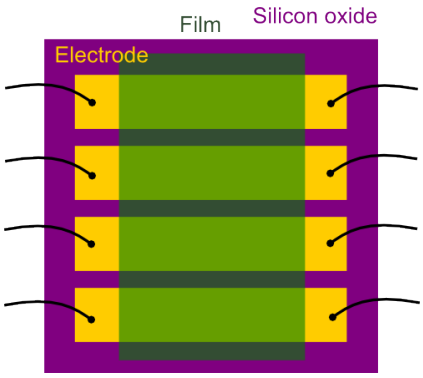

(a) Top view

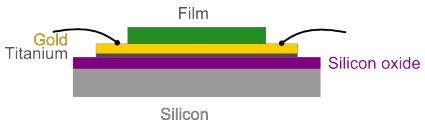

(b) Side view. The layer thicknesses are not in scale - oxide layer is about hundreds of nanometer, Ti 3 nm, Gold 12 nm and film a few tens of nanometers.

Figure 10: Sample structure.

evaporation. The mask had three thin copper wires drawn over a frame which left gaps to metal layer separating electrodes from each others. After evaporation lift-off was made in acetone which removed the PMMA and left the edges clean. Ending the electrodes further from chip edges ensured that there would be no contact from electrode to silicon core. Sometimes, when the chips are broken from pre-cut wafer, the edges are not straight and the oxide may be damaged.

4.2 Hydrophilicity treatment

Surface of the chip was made hydrophilic with reactive ion etching system (RIE). Oxygen recipe with 30 W power and 40 mT magnetic field was run 30 seconds. During the process some oxygen attaches to the surface. A polar water molecule attaches easier to polar oxygen ion than to non-polar silicon oxide. When the surface rejects the deposited droplet less, the wetting improves which shows as a decrease of contact angle. The effect of hydrophilicity treatment does not last long in room air and the sample should not be left laying around or the effect will be soon lost.

4.3 Film deposition

CNT-cellulose films were made on top of the chip's basic structure. Double-walled carbon nanotubes (DWCNT) and hemicellulose were dissolved to water. The nanotubes were from Unidym and used hemicellulose was xylan . The CNT-cellulose weight ratio was 1:1. We did not prepare the solution ourselves but it was provided by nEMCel Ltd.

Small amount of solution was deposited on the chip by spreading with pipette tip or by spinning. Different methods were used to search for ways to control the film thickness. Also hydrophilicity treatment's effect with different deposition techniques was tested.

In pipette deposition a big droplet was spread over the chip. The droplet was spread so that it covered as big area as possible. Still the edges of the chip were left clean to avoid the collapse of the deposited droplet. We tried to control the film thickness by estimating the height of the deposited droplet

Table 1: Table showing the fabrication details of different samples. Hydrofilicity column shows if hydrofilicity treatment was done before film deposition.

Sample	Hydrofilicity	Solution concentration and deposition method
AJ1	+	50 ppm, dried droplet
AM1	+	100 ppm, 1500 rpm spinning
AM2	+	100 ppm, 1500 rpm spinning
AM3	+	100 ppm, 1600 rpm spinning
AN1	-	100 ppm, dried droplet

and also by weighting the droplet. Some of the solution of the droplet could be sucked back by pipette and still be able to obtain the achieved wetted surface area.After deposition the chip was left in fume hood to dry for a day.

Many parameters were tested with spinning produced samples. We managed to adjust the film thickness on clean and smooth silicon oxide surfaces by changing the spinning speeds but not as clear resemblance was seen with samples that had electrodes. Because the electrodes rose from the surface they changed the behaviour of a droplet. Hydrophilicity treatment was used to ease the spreading of the droplet but the outcome with electrodes was not easy to control. A droplet was deposited on a sample right before spinning. Spinning speeds of ~1500 rpm were used in 60-90 second runs. At times the sample was still wet after spinning and it was spun again. This was repeated until there were just little droplets in the corners of a chip and then it was left to dry in fume hood.

The fabrication differences between samples is shown in table 1. Sample AN1 is an exception as we wanted one clearly thicker film for comparison. AN1's film deposition started by depositing a big droplet without hydrophilicity treatment. After the first droplet had dried a second droplet was deposited on the existing film for clearly thicker outcome.

Samples of this report were made in clean room. The chip surfaces were clean before film deposition which means that possible contamination would be on the top surface of the film after the sample has left cleanroom. The AFM imaging after depositions rarely showed big impurities which would propose also clean CNT-cellulose solution.

4.4 *Cleaning the film edges*

Deposited films covered the whole surface of the chip. The films, made by drying, had clearly darker edges which brought to mind coffee stains. The edges of all samples were always wiped clean for more uniform film. Wet cotton sticks were used to cleaning. Wet cotton was not that accurate so often a wooden end of the cotton stick was carved thin, dipped in water and then used to clean the areas. This left the edge of the film sharper. Figure 11a has on left a film on glass, done by drying a droplet. Its sides have been cleaned and coffee stain like markings can be seen on upper and lower parts of the film.

In figure 11a on right is two more samples on silicon chips. All the edges of those samples have been clean to ensure that there is no contact over the edges to silicon layer of the substrate. Also the ends of the golden electrodes were cleaned for better contacts for aluminium wires. Most uniform part of the film, the center, was left for measurements.

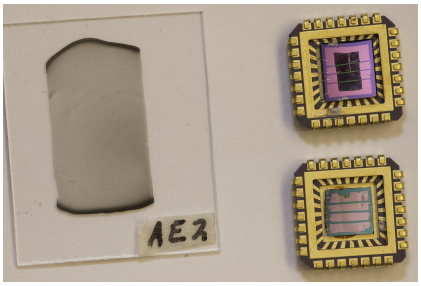

(a) On left a film on glass substrate showing the transparency. On right two samples made on silicon and glued on carriers. The right ones have different film thicknesses, 100 nm on top (AN1) and 12 nm on bottom (AJ1), which can also be seen from the shade of the film.

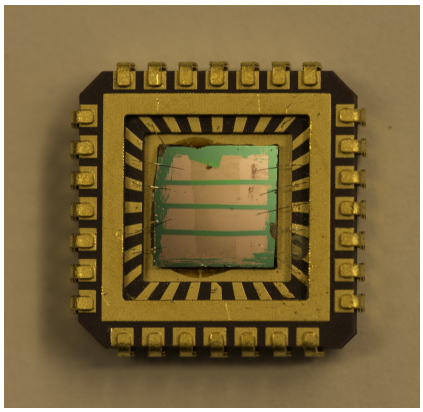

(b) Image of sample on carrier. The same sample as in lower right corner of image (a)

Figure 11: Photographed samples.

4.5 Chip carrier

Specific chip carrier was needed in low temperature setup. Sample chip was glued on the carrier and electrodes of sample were connected from the cleaned area to the electrodes of the carrier (fig. 11b). Electrode connections from chip to carrier were bonded with aluminium wire. Bonding required extra attention because the needle of the bonder broke the thin, insulating oxide layer of the chip easily if settings were wrong. Such break would enable current leakage to back gate.

Two connections were also done from the electrodes of the carrier to silicon layer of the chip. The wire was bonded close to the edge of chip and silver paste was used to create contact to silicon layer revealing on the side of the chip. The paste droplet was spread over the edge to cover the wire and the side of the chip. The paste must not touch the electrodes or there would be leakage to back gate. Two contacts to back gate were needed to assure its functionality.

5 Imaging

Imaging was one of the first things to do as we begun with a new material. In figure 11a (page 16) is shown what bigger film looks like on glass. If looked carefully one can see that the film is not perfectly uniform, not even in the middle.

The first images were taken on optical microscope to see the film little more detailed. It showed immediately the roughness of the film (fig. 12). The film was clearly transparent throughout but not perfectly uniform. Material seemed to form dunes that made film look scarred or wrinkled. Also some samples had minor holes in the film which may have come during sample fabrication or just by random alignment of very thin film.

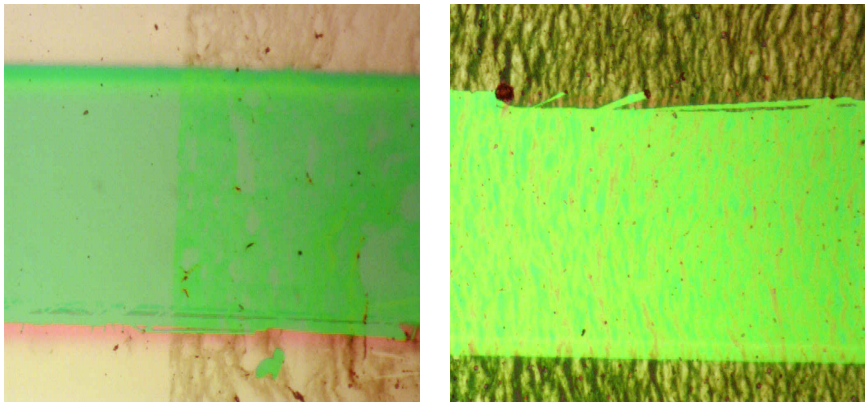

(a) Golden electrodes on top and on bottom, gap in between. Cleaned area on left and film on right.

(b) Cellulose-CNT film covering electrodes and a gap between them.

Figure 12: Films imaged on optical microscope. Roughness of the film is easily visible.

The next step was to image the film with AFM. We were interested in the alignment of the fine structure although the CNTs and cellulose would look the same. The pattern showed out very quickly – there was random fiber network pointing here and there as expected (fig. 13).

Surprising ring formations were seen on AFM images. Those rings were visible all over the film and on every sample. The diameter of the rings varied

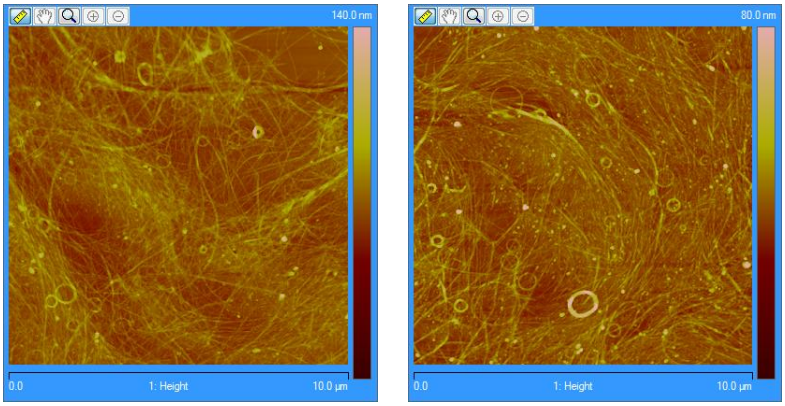

(a) **(b)**

Figure 13: AFM image from average film of measured samples.

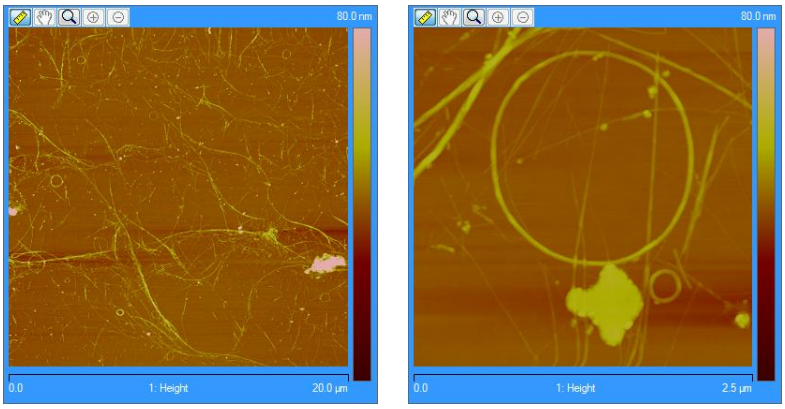

(a) Thin and non-continuous film.

(b) Ring formation magnified on AFM.

Figure 14: Thinner film for AFM imaging of ring formations.

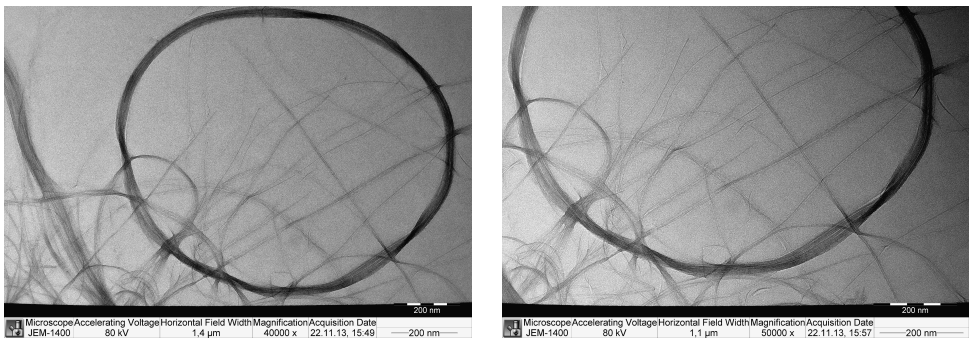

(a) **(b)**

Figure 15: TEM images from a ring formations.

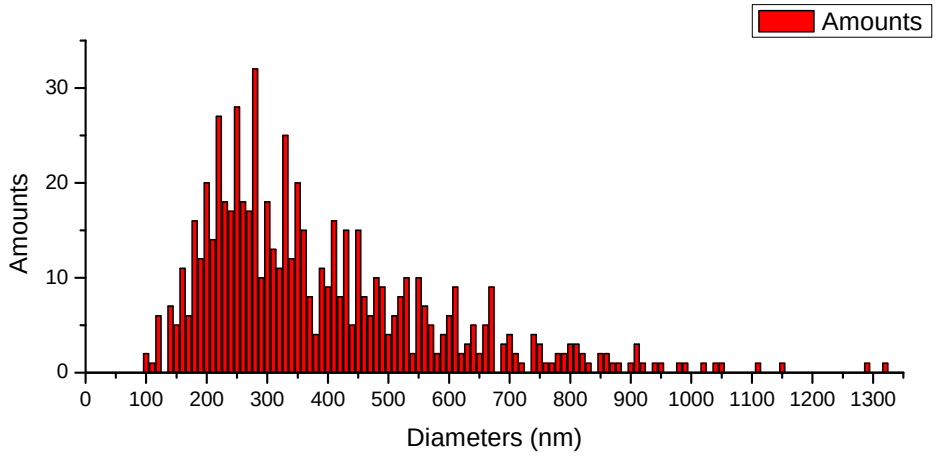

Figure 16: Distribution of ring diameters. The smallest rings got easily lost in the fiber network.

a lot and statistics about that diameter distribution is shown in fig. 16. Very thin and non-consistent films were made for more detailed AFM images of the ring formations (fig. 14).

The resolution of AFM could not show detailed structure of rings (fig. 14b) so transmission electron microscope (TEM) was used. TEM images in figure 15 show a ring in more detailed. They look like microscopic coils as there is several loops per ring. However the ends of the tubes could not be seen in rings. The rings were traced back to the CNT material and their formation has nothing to do with hemicellulose.

5.1 Measuring film dimensions

As mentioned, the film was more uniform in the middle so edges were cleaned and thickness was measured on AFM. Because of the surface roughness averaging was used.

Example from the height averaging of AFM software is shown in figure 17. On left side of the image the averaged area is chosen by limiting it inside the big, white-dashed rectangular. Height average is calculated for each vertical column of pixels. The middle vertical dashed line could be considered as cutting line for side view that is then represented on the upper right

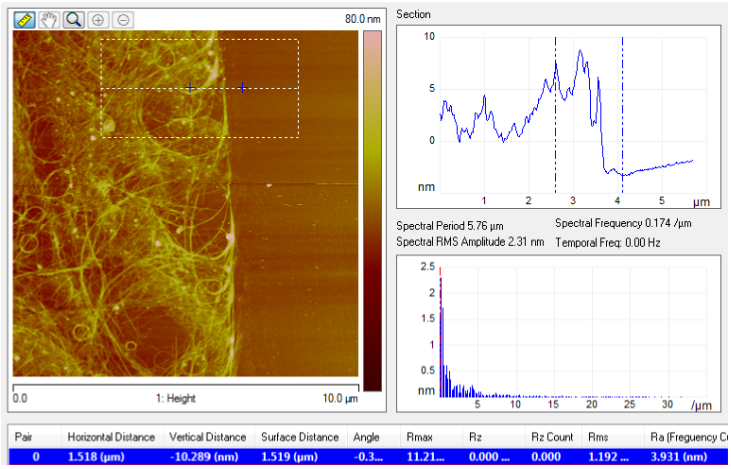

Figure 17: Averaging of AFM software, used to estimate the film thickness. On left is the height profile of a film from which an area is chosen by limiting it with white, dashed rectangle. Averaged height profile of the chosen area is shown on top right as a side view profile.

corner as graph. In that graph there is two vertical lines that can be used to select certain points for comparison. One point was selected from smooth, clean surface and an other one from some average looking part on film. The software showed the comparison of points in table that can be seen in the very bottom of figure 17. From the table the thickness can be read and it's about 10 nm in this case. The height profile in upper right corner is clearly tilted so little fixing was done to thickness reading. The slope was estimated on the smooth area and its effect was added to the thickness estimate.

Smooth and average looking areas were chosen for thickness estimation. The four probe measurement defines the conductivity of the middle gap (fig. 2) so we focused on the thickness of the middle section. We tried to take images from that film section's both edges and also from middle. Some times we could find very small areas in the middle where the substrate was visible and that could be used as a reference to estimate the film thickness. Averaging the thicknesses of different areas was used to define the final film thickness.

AFM did not suit for thickness measuring of sample AN1. We had noticed with thicker, droplet deposited films that the edges of the film rise higher than

Table 2: Film dimensions of different samples at the middle gap crossing section. Thickness is average from AFM images and the others are measured on optical microscope with a scale. Error for optically measured values is estimated to 5 %.

Sample	Thickness (nm)	Length (µm)	Width (mm)
AJ1	12.1 ± 1.0	440 ± 30	1.84 ± 0.10
AM1	25.3 ± 1.5	200 ± 10	2.42 ± 0.13
AM2	7.3 ± 0.6	115 ± 6	1.38 ± 0.07
AM3	13 ± 2	90 ± 5	2.50 ± 0.13
AN1	94 ± 5[†]	115 ± 6	2.60 ± 0.13

the middle making the side profile look like a crater. Also cleaning of the edges pushes the wiped film in front of the cleaning tip. When the cleaned film piles up, some of it falls on the remaining film and locally increases the thickness. That would have given misleading height reading from the edge. In the middle there would not be any reference height where to compare the height difference between film and substrate.

We decided to measure thickness of AN1 with profilometer. The sweep of the profilometer was long enough to travel all across the sample chip. Thickness profile included sections from the clean parts of chip before and after film. Those clean areas were used to calibrate the thickness profile. The film was thicker and rough on the edges so the middle section was used for thickness reading. Again averaging over smooth area was used to get the reading.

For conductivity calculations also the width and the length of the film were needed. For those we used optical microscope which had a scale drawn on its objective. Those readings were converted to actual measures with supplied conversion table. All the results of dimensions measurements are in table 2. For AFM defined thicknesses error comes from the standard error of mean, because overall thickness was average of local thicknesses. For other dimension measurements the thickness is estimated to 5 %.

[†]Measured with profilometer and error was estimated to 5%.

5.2 Discussion

AFM and TEM imaging showed nicely the fine structure of film. Fiber network was expected and it resembles the film reported by Koga et al.[16] The only difference in images is that Koga et al. had finer fibers due to thinner SWCNTs and shorter cellulose fibers. Imazu et al had made thin films, very similar to ours, out of DWCNT and sodium carboxymethylcellulose (CMC).[17] Their AFM images look like their films are thinner and consist of straighter fibers which are less bundled. The structural difference is most likely comes from their ultracentrifugation of CNT matrial which was used for purification and obtaining longer tubes.

After all our structure was surprisingly similar to pure CNT networks.[1, 18–20] Common problem with CNT films is the bundling of the CNT which is prevented with various dispersants/surfactants or solvents. In our film the cellulose plays the role of the dispersant making the CNT soluable to water and helps to keep tubes separated. Other kind of cellulose, sodium carboxymethylcellulose (CMC), is also known to be excellent dispersant for aqueous CNT solutions[21] but also a way to purify the CNT material.[8]

CMC was also used as dispersant by Tenent et al.[22] to produce SWCNT films but the cellulose was removed from the final film with acid treatment. They reported also transparent film but ultrasonic spraying technique was used. The same technique might be tried also with our material to test if it gives more uniform surfaces but this technique becomes even more compelling if bigger films are made. Tenent et al. had made their films onto oxygen-plasma-cleaned glass which is basically the same as our hydrophilicity treatment but they have not mentioned how soon after the treatment deposition was done. Some of the oxygen of the plasma sticks to the substrate surface leaving the surface more hydrophilic but that only lasts for some time. For thicker films Meyer rod coating[23] or Langmuir–Blodgett deposition[24, 25] might be more suitable but as the film thickens the transparency is quickly lost.

As it was seen in optical images (fig. 12) the film looks wrinkled. This roughness must come from deposition and some solutions to overcome that

is represented in previous paragraph. The roughness also gives some error to the film thickness measurement. As thickness values are used in calculation of other values the error will add up.

The ring formations and their commonness in the film surprised us. Their existence became known in the end of 1990's.[26–29] At first it was not known if the rings are formed from one tube where the ends are covalently connected to each others (carbon nanotori) or if the van der Waals forces bind the tubes to coils[‡] which might be considered as bundling. Ways to produce rings from different nanotubes with various diameters have been found and DWCNT rings are known to be bundles.[30,31] We don't know exactly how big role the rings play in big picture but as they resemble microscopic coils, some reactivity to magnetic fields could be expected.

There has been no research about these CNT rings in thin films at the time of writing. Theoretical predictions have been made on carbon nanotori's persistent currents[32] and paramagnetic moments.[33] Experiments have been made on individual SWCNT rings considering low-temperature magnetoresistance[34] and electronic field emission.[35]

There has been research on CNT materials as electro magnetic interference (EMI) shields[36–38] (frequency scale MHz–GHz). That was also the main application for this material in the beginning of the development. Some EMI shielding measurements have been made in which this material showed good results and it might have something to do with the coils.

[‡]Name 'coiled CNT' is often used for spiral CNTs which are a different case.

6 Conductivity

Carbon nanotubes have been widely used in various composite or hybrid materials to increase the electric conductivity of the material. Our film was know to be conducting and some essential electric quantities were defined. We also examined how the environment effects to electric properties.

The first step was to define the conductivity in average room air. The measurements were done using circuit of figure 18. Constant current was applied via resistor trough the outermost electrodes while the voltage difference between the middle electrodes was measured. The current was applied about 30 sec to get average of current and voltage readings which were then used to calculate the resistance over the middle gap. Offset of these meters was fixed by gathering the reading with current switched off.

We did a few resistance measurements per sample where the test currents varied from 1 µA to 100 µA. The resistances in table 3 are averages of these different measurements and error is taken as error of average.Conductivity and surface resistivity were derived from resistance values using the dimensions of film (table 2). Error estimation of conductivity and surface resistivity was done with the propagation of error because the resistance and the dimensions had their own errors which add up to result.

Sample AM1 stands out from the others with order of magnitude better conductivity. AM1 is the thickest which might result the best conductivity. There might be a trend that the conductivity saturates after certain thickness as it has been with some SWCNT networks.[39] We had also prepared one significantly thicker sample which showed lower conductivity than AM1 so

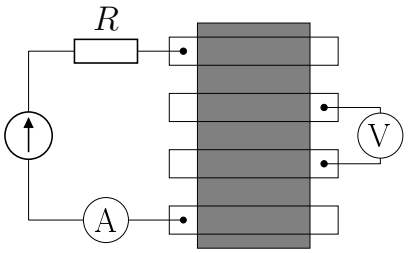

Figure 18: Four probe measurement circuit used with the samples.

Table 3: Measured electric properties of samples in room air conditions. Samples are the same is in table 2.

Sample	Resistance (Ω)	Conductivity (S/cm)	Surface resistivity (Ω/sq.)
AJ1	1403 ± 3	140 ± 20	5 900± 600
AM1	19.8 ± 0.3	1600 ± 200	240± 20
AM2	543.9 ± 0.7	210 ± 30	6 500± 500
AM3	224.1 ± 0.9	120 ± 30	6 200± 500

more likely AM1 is a very successful sample. On the other hand it was seen in imaging that the fabricated film was rarely uniform which might explain variation between samples.

To compare other reported values, Imazu et al.[17] had very similar film but their cellulose was CMC and their best sample had the surface resistivity of 320 Ω/sq. with DWCNT:CMC ratio of 1:1. At the time of writing there was no other reported results about DWCNT cellulose films and we had to compare our results to some similar materials. Best conductivity or surface resistivity results (in room air conditions) found with CNT based films were:

- vacuum filtered SWCNT-cellulose film: 174 S/cm
  Mahiar M. Hamedi, Alireza Hajian, Andreas B. Fall, Karl Håkansson, Michaela Salajkova, Fredrik Lundell, Lars Wågberg, Lars A. Berglund. Highly Conducting, Strong Nanocomposites Based on Nanocellulose-Assisted Aqueous Dispersions of Single-Wall Carbon Nanotubes. *ACS Nano,* 8(3):2467-2476, 2014. PMID:24512093

- DWCNT network: 146Ω/sq.
  Alexander A. Green and Mark C. Hersam. Processing and properties of highly encriched double-wall carbon nanotubes. *Nature Nanotechnology,* 4:64–70, 2009

- thionyl chloride doped DWCNT film: 40 Ω/sq.
  Alexander A. Green and Mark C. Hersam. Processing and properties of highly encriched double-wall carbon nanotubes. *Nature Nanotechnology,* 4:64–70, 2009

- transfered SWCNT network: 2 000 S/cm (or 200 Ω/sq.)

Yangxin Zhou, Liangbing Hu, George Gürner. A method of printing carbon nanotube thin films.*Applied Physics Letters,* 88(12), 2006.

- acid treated SWCNT network: 5 500 S/cm (or 40 Ω/sq.)
  Hong-Zhang Geng, Ki Kang Kim, Kang Pyo So, Young Sil Lee, Youngkyu Chang, Young Hee Lee. Effect of Acid Treatment on Carbon Nanotube-Based Flexible Transparent Conducting Films. *Journal of the American Chemical Society,* 129(25):7758-7759, 2007. PMID:17536805.

- superacid dispersed SWCNT film: 12 825 S/cm (or 60Ω/sq.)
  David S Hecht, Amy M Heintz, Roland Lee, Liangbing Hu, Bryon Moore, Chad Cucksey, Steven Risser. High conductivity transparent carbon nanotube films deposited from superacid. *Nanotechnology*, 22(7):075201, 2011.

As it comes to cellulose materials, our best sample seems to be among the best. In later measurement we have achieved even higher conductivity for the sample AM1 (table 5, p. 40).

Indium tin oxide (ITO) is nowadays widely used transparent conductor which can reach conductivities higher than 12 900 S/cm.[40] Due to the depleting indium resources alternative materials are researched. According to listing above CNT based cellulose films fall behind the acid treated- and bare CNT results so the composites are less likely to replace ITO in industry. Greatest advantage of CNT films over ITO is the bendability. Many CNT thin films can take bending – composite film or pure CNT network. Depending on application the bendability can overweight the conductivity. In addition our material is fairly easy to deposit compared to sputtering of ITO. Also graphene based solutions have been researched to replace ITO [41] so the future of carbon based electronics seems promising.

To further improve the conductivity of our film, acid treatments or doping could be considered. Acid treatments dope the tubes but atleast damage, if not destroy, the cellulose component and then the advantages of cellulose are lost. At the moment the xylan is only known to disperse the tubes to water but there has been no experiments to remove the cellulose from final film. There is always room for fine tuning of properties in various applications. At

the beginning the major application for our film was EMI shielding where the conductivity is related to shielding efficiency but it is not the only factor. Transparent, easy to deploy shielding material surely has market too if other materials are better for optoelectronics.

6.1 Cooling and low temperature

Measurement setup, introduced in section 3.1, was used to cool down the sample. Circuit of figure 18 was used with 10 µA currents on all the samples. Offsets of meters were defined before cooling by collecting readings without applying the current.

Measurement was started before the chamber of dip-stick touched the liquid helium level and was left running. Once the readings seemed stable dip-stick chamber was sunk in liquid helium and cooling started. Conductivities of different samples were plotted as function of temperature and are shown in figure 19.

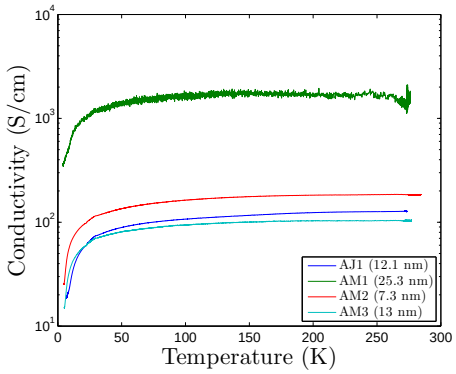

(a) Values of conductivities.

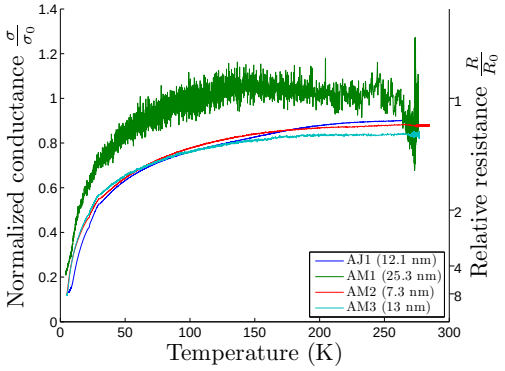

(b) Normalization values σ_0 and R_0 from table 3

Figure 19: Conductivities of samples during cooling.

Although the samples have different conductivities they all follow the same trend in cooling. The comparison of samples was made easier by normalizing the conductivities of cooling with the room temperature value of each sample (table 3). Final adjustments of setup were done while the sample was waiting in upper part of the dewar. By the time of starting the

measurement the sample had slightly cooled down so each cooling measurement had a bit different starting temperature. By normalizing with room condition value, we could take normalization values that have common conditions although the environment of normalization was room air and in this measurement it was low pressure helium.

The conductivities drop with the temperature but slowly. As temperatures drop below 50 K the conductivity dependency becomes more significant. Any CNT-cellulose films were not found for comparison to our cooling results but some similar research has been done with SWCNT networks. In some researches SWCNT networks have local maximum of conductance on range 150-200 K.[5, 42] Similar minor local maximum can be seen with AM1 but not with the others. It could be possible that even the cellulose drops the conductivity, compared to bare CNT, it also stabilizes it by being more immune to small changes of environment.

6.2 I-V behaviour

Some carbon nanotubes are known to have non-ohmic behaviour. This phenomenon shows clearly in low temperatures. The conductivity's dependency on applied current and voltage was tested with our material in room temperature and in 4.2 K.

I-V behaviour was observed with two different measurement circuits. First circuit was with current source (fig. 18). Different test currents were applied in constant conditions while the voltage and current readings were gathered for a while. Resistance was calculated from the averages of those readings. Test currents were varied in room temperature but also in low temperature and the results are shown in figure 20.

Figure 20 shows that the conductance of film does not depend on applied currents in room temperature but in low temperatures the case changes. For more continuous graph we used slightly modified circuit which is shown in figure 21a. In these measurements the applied voltage U swept a loop while the readings were gathered. I-V values were plotted (fig. 21) and resistance values of different voltages were derived from the slope of the curve. Slope

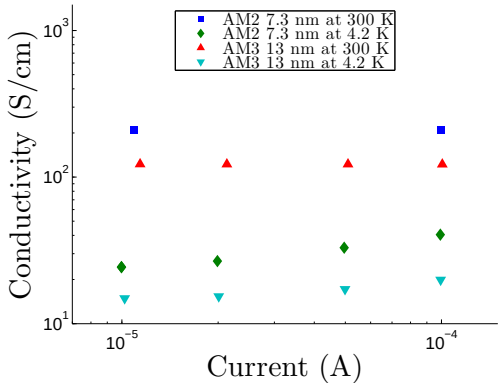

Figure 20: Conductivities of two samples as function of applied current in 300 K and in 4.2 K.

was defined by using linear fit to a point and its 10 nearest neighbours on both sides. Resistance values, combined with film dimensions, were used to derive the conductivity values which are plotted as function of voltage (over the middle gap) in figure 21 also. The same measurement was done in room temperature and in 4.2 K.

In low temperature the material clearly shows non-ohmic behaviour as the bias increases. This might be result of electrons exiting to states of better conductivity due to bias or due to heating of the film. We had already seen that in low temperatures conductance strongly depends on temperature. Heating of the film can not be proven because the temperature sensor was next to the sample and not measuring the temperature actually from the film. When temperature and voltage were compared as function of time, there is minor changes in temperature but less than one kelvin changes are most likely just noise.

Setup arrangements bring some uncertainty to results as the 300 K measurements were done in normal room air environment but the low temperature measurements had low pressure helium environment. The film's conductivity has seemed stable in low humidities and in helium environment so temperature is assumed to be the cause of results. In future it would be recommended to test the films reaction to different gasses.

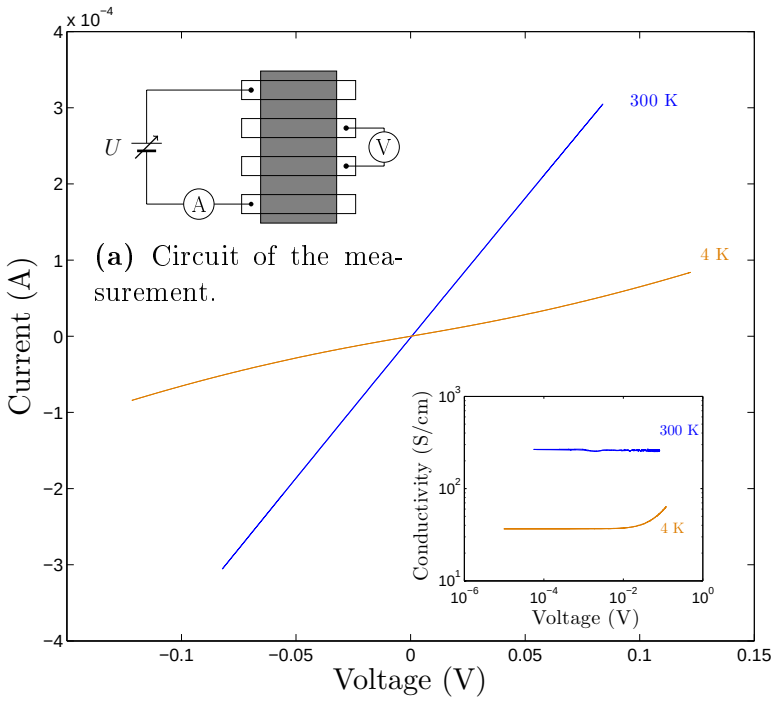

(a) Circuit of the measurement.

Figure 21: I–V curve in room- and low temperature. Conductivity was derived from the slope and drawn to smaller graph. Sample was AM3.

6.3 *Back gate response*

Carbon nanotubes can be divided to metallic and semiconducting. These properties are dictated by chiralities of the tubes. With MWCNTs the nature of the whole tube is out come of different layer chiralities and their interaction. There is both metallic and semiconducting DWCNTs.

Building samples on oxidized silicon made gate voltage sweeps possible. The circuit schematics is shown in figure 22. These measurements were done in 4.2 K because there mostly the lowest energy states would be occupied and the possible change of conductivity would become clearer upon excitation. We did not notice any significant change in conductivity as the back gate voltage was swept between −15 and 15 V. Unfortunately we were able to do this measurement only to sample AM3 as the others had problems with the oxide layer. If there is current from back gate to the film the measurement fails.

The results show that the film contains atleast metallic carbon nanotubes. Absence of semiconducting tubes cannot be declared but there is no proof of their existence in the material either. Transistor applications do not seem likely for our material but DWCNT transistors have been made from individual tubes[43, 44] and from networks.[45] For thin film transistors SWCNTs seem to be better material[45] although DWCNT can have semiconducting properties too.

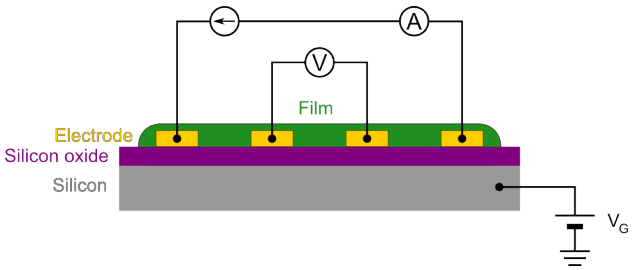

Figure 22: Circuit of back gate connection.

6.4 Theoretical models of electron transport

The cooling data was plotted according to different models on whole temperature range. When the axises of plots are chosen appropriately, the sections fitting the model show linear. The VRH model (eq. 3) can be formulated as

$$\ln \sigma = (-T_0)^{\alpha} \cdot T^{-\alpha} + \ln \sigma_0 \qquad \text{, where } \alpha = \frac{1}{d+1}. \tag{5}$$

When $\ln \sigma$ is plotted as function of $T^{-\alpha}$, the plot resembles linear function. The fitting of all data in 2D and 3D case can be seen in figures 23a and 23b. Same sort of fitting was done also to FIT model where the equation 4 can be formulated as

$$\left[\ln\left(\frac{\sigma_0}{\sigma(T)}\right)\right]^{-1} = \frac{1}{T_1} \cdot T + \frac{T_0}{T_1}. \tag{6}$$

The FIT plot is in figure 23e. Sample AM1 was left out from fig. 23e because of the noisiness of the signal.

Plotted data of each model has a few linear sections. Widest possible temperature range was chosen so that all the samples had linear behaviour in it and linear fitting was done. For both VRH models the range was 27 – 180 K and for FIT model 27 – 150K. Based on the widths of the temperature ranges, VRH seems to apply better. Dimensionality of the VRH model does show significant difference in plots (fig. 23c and 23d).

When the whole temperature range is considered on each model, the ranges can be split to a few sections which all can be estimated separately as linear. Fitting same model with different constants on various ranges wrecks the theoretical background but two different sections can be estimated with different models.[46] As mentioned VRH applied better on temperature range 27 – 180 K but in addition FIT works well on temperatures 7 – 32 K. On these ranges the constants of models were derived from the linear fitting (fig. 23c,d and f) and they are shown in table 4. OriginPro software was used for fitting which gave error for fits and propagation of error was used to derive errors of the constants. Error estimations were made to all thou the errors of temperatures seem unrealistic.

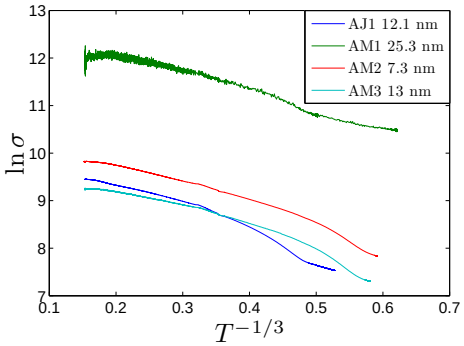

(a) 2D VRH model applied on whole measured temperature range.

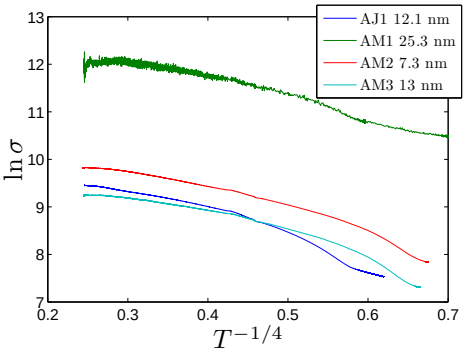

(b) 3D VRH model applied on whole temperature range.

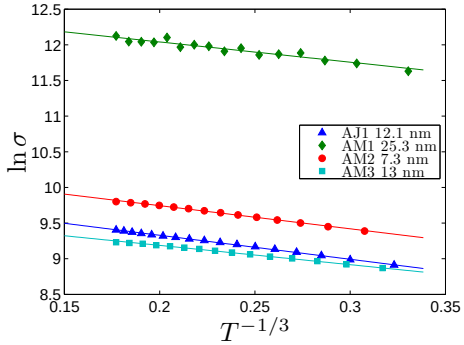

(c) 2D VRH model fitted on 27 – 180 K.

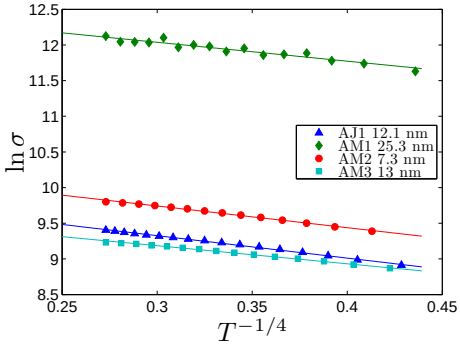

(d) 3D VRH model fitted on 27 – 180 K.

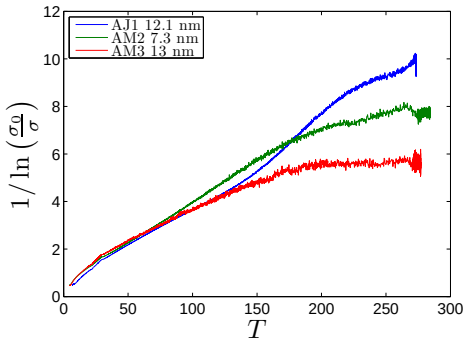

(e) FIT model applied on whole measured temperature range.

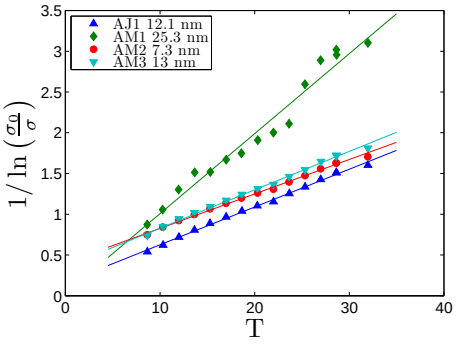

(f) FIT model applied on lower temperature range: 7 – 32 K.

Figure 23: Graphs from fitting the cooling data to different models.

Table 4: Sample specific constants of different models derived from linear fittings.

Model (Temp. range)	Constant	AJ1	AM1	AM2	AM3
2D VRH	T_0	38.107±0.011	22.8±0.5	34.18±0.10	19.75±0.07
(27 – 180 K)	σ_0	22 070 ± 20	298 600 ± 1 500	32 640 ± 30	16 780 ± 12
3D VRH	T_0	98.0±0.6	49.2±1.5	85.4±0.5	41.3±0.3
(27 – 180 K)	σ_0	28 850 ± 50	374 000 ± 3 000	42 360 ± 60	20 860 ± 30
FIT	T_1	21.57±0.02	10.19±0.06	23.66±0.08	21.22±0.06
(7 – 32 K)	T_0	3.493±0.008	0.27±0.1	9.56±0.08	7.58±0.07

6.5 Humidity

The films were made from water solution so it was expected that humidity would have some effect on the film. The setup to control humidity is described in section 3.2. We used same circuit as in figure 21a and the measurement was run when stable humidity was reached. Resistance was derived from the slope of I-V curve using linear fitting and conductivity was derived from the resistance.

Results are shown in figure 24. The humidity was first increased from zero to maximum and then decreased to minimum. In the graph the loop begins in left end of upper branch and next data points continue to right and then back to left along the lower branch. The conductivity slowly starts to drop as the humidity increases. Around relative humidity of 60 % the conductivity begins to drop faster. When the humidity is decreased, the conductivity slowly improves except with sample AJ1. Conductivities did not return to initial value after the measurement loop on any sample.

There is some trend visible in figure 24a. The changes of conductivity were not in orders of magnitude and the relative changes ease the comparison of samples. The first measured value of a sample in these humidity experiments was used to normalize all the other values of a sample. The values of table 3 were not used as films had gone through consuming measurements and the conductivities had changed. Mainly the normalized conductivity does not drop below 50 % with the stabler samples. The humidity clearly has weakening effect on conductivity but the conductivity recovers by drying.

Hysteresis proves that there is some delay on films reaction to the change

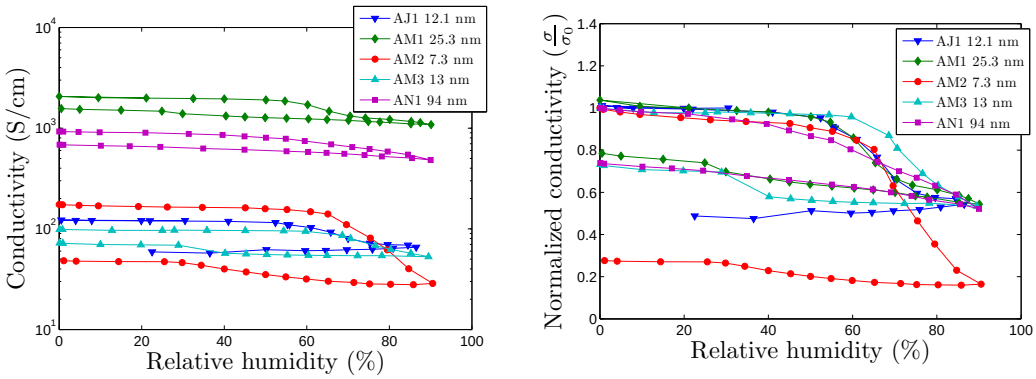

(a) Conductivity values

(b) Conductivities of different humidities (σ) normalized by the first value of humidity experiment (σ_0).

Figure 24: Conductivities of different samples as function of relative humidity. In time order the measurement points go from the left end of upper branch to right and then back to left along the lower branch.

of environment. The self-build setup was difficult to adjust and time between data points varied from 5 to 25 minutes. If the system was left to stabilize even longer times the hysteresis could be smaller. Hysteresis also suggests that the water molecules absorb deep in to the film. If the water only attached to very surface of the film the conductivity would return quickly to the initial value.

In molecular level the absorbed water molecules could rearrange the fiber network structure. Absorbed water molecules would push the fibers further apart. As the concentration of CNT drops their contacts become rarer and tubes lay further from each others. This understandably would decrease the conductivity. If absorbed humidity does not remarkably change the binding of cellulose the conductivity should return to initial value when the water content of film returns back to initial level.

Now we measured the humidity of the environment, not directly the humidity of the film, so the final humidity of the film may have been higher than the humidity of the dried environment. It would be interesting to see how long it takes from film to completely recover from humid environment. Totally dry film would also work as better comparison point than in room

air stored films.

The samples AJ1 and AM2 stand out from the others by the biggest relative change of conductivity. They happen to be the thinnest samples. AJ1 probably differs because it was made from different solution. The significant drop of AM2's conductivity is exceptional and suggests something more dramatic change such as partial dissolving of film. The change of humidity could also make the film wrinkle causing smaller contact area on electrodes and resulting to weaker conductivity. The heating experiments (next section) followed the humidity experiments and the first heating of AM2 improved it's conductivity but it still stayed clearly weakened compared to first measurements so the humidity had some permanent changes to the film.

Because the conductivity was derived from linear fit of the I-V curve we needed to check the ohmic behaviour again. The conductivity of all samples stayed constant at applied voltage range during each humidity point so the linear fit was acceptable approach. Compared to measurements of section 6.2 the applied voltages were smaller and on scale of image 21 these measurements would be on range of constant conductivity anyway.

6.6 Heating

In many electronic devices the circuits heat up. Depending on application the temperature can rise above 100 °C. Stability of our film's conductivity was tested in temperatures above room temperature. The setup is described in section 3.3. Upper limit of temperature was set by the melting point of soldering tin which was used in contacts of measurement box.

The heating experiments gave very mixed results. Each sample was heated four or five times to prove pattern. Not even all the heating runs of one sample gave same results. Result of a heating run on sample AM1 was chosen to be shown as the sample had most promising conductivity based on earlier experiments but also it seemed to repeat same behaviour on each heating. AM1's results are shown in figure 25a. The conductivity increases with the temperature as long as the sample is heated. When the heating stops and we tried to keep constant temperature, the conductivity starts to

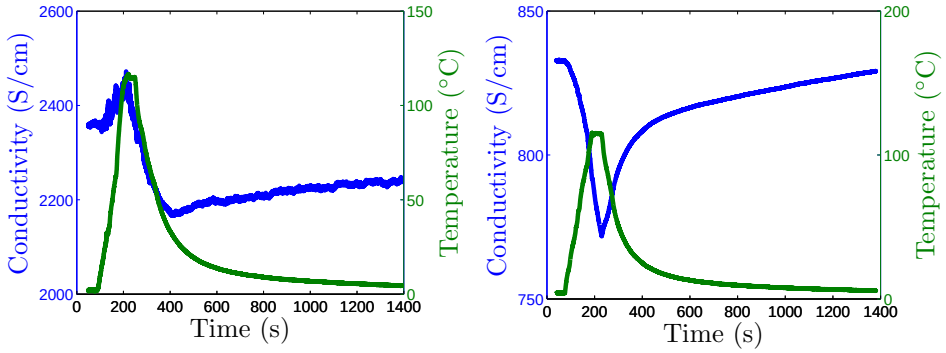

(a) AM1 **(b)** AN1

Figure 25: Response of different samples to heating.

decrease suddenly. When cooling starts there is a minor peak in changing conductivity but still it keeps decreasing. After the samples has cooled down a while the conductivity improves again but only very little. The same trend was seen in each heating experiment of AM1. The repeatability of the results, which was not obvious on all samples, may come from the thickness as thicker film reacts slower to change of environment, meaning more stable behaviour.

Other sample which had consistent reaction to heating was AN1 and it is shown in figure 25b. The response to heating was very different from AM1. AN1's conductivity started to drop as the heating started and kept on dropping even when the high temperature was kept constant. At the point of cooling down the conductivity slowly started to return close to the initial value.

We tried to figure out different explanations how the heating effects to the samples. Nothing we considered relating to doping water molecules, thickness or derivative of temperature could explain the contradictory results. To put all the results in perspective the conductivity usually varied less than 15 % during the heating. That means fairly stable conductivity in many applications. The same kind of stability was also seen in cooling measurements (section 6.1). To examine the heating process in detailed more sophisticated setup is needed.

6.7 Discussion

Conductivity of the film seems very promising. The best sample has higher conductivity than any other CNT-cellulose material reported at the time. The conductivity seems to remain in 15 % tolerance on wide temperature range of approximately 100 – 400 K and endures humidity changes up to 50 % RH with similar tolerance. Good conductivity combined with stability and transparency make this material desirable in many applications.

The fabrication technique needs to be fixed to produce more homogeneous samples. The conductivities of samples had variance and one sample stood up from the others. Different recipes should be tested so that the quality can be optimized and reproduced.

Although the samples had differences, their behaviour was mostly similar. In cooling and humidity experiments clear pattern was visible. On the other hand heating experiments should be repeated with more sophisticated setup as the results between the samples differed so much that nothing could be concluded for sure.

In 4.2 K non-ohmic behaviour was noticed and the film did not show semiconducting properties. These experiments give a peek to charge transport which we tried also explain with theoretical models. FIT model worked well in 7 – 32 K and VRH covered 30 – 180 K. Similar behaviour has been seen with CNT networks[46] so the cellulose component does not have that big effect on charge transport.

Samples have gone through a few measurements which must have had some effect on the samples. This can be seen as slowly changing conductivity in different measurements. All the measurements have been done to each sample in the same order and the changes can be seen in table 5. At first already the vacuum had some effect on samples (beginning of cooling measurements). In vacuum the humidity of a sample should drop but opposite change suggests that gasses of the environment might have some effect also.

The samples recovered from cooling experiment reasonably well. Small drop of conductivity occurred except on AM1. Explanation for different behaviour could come from the thickness – the thickest film had not dried

Table 5: Conductivities of samples in different measurements. The values of three last measurements are at the beginning of a measurement (upper) and in the end (lower).

Measurement	Sample conductivity (S/cm)			
	AJ1	AM1	AM2	AM3
Room air	140	1600	210	120
Cooling	130	1600	190	100
	20	350	26	15
Humidity	120	2000	170	100
	58	1600	48	72
Heating	150	2400	130	110
	150	2100	130	100

as well as the others but then the improved conductivity should be seen already in vacuum. Anyhow the low temperature measurement improved AM1's conductivity significantly but the cause is unknown.

Humidity clearly dropped the conductivity of all samples. The samples AJ1 and AM1 recovered well from humidity measurement to heating experiments and their conductivity actually improved compared to initial room air measurements. This could suggest some kind of self repairing effect if the absorbed humidity rearranges the fibers. AM3's conductivity also recovered well after humidity but it settled a bit below the first room air measurement. Totally opposite reaction was seen with AM2 which was the thinnest sample. Dramatic weakening was seen already in high humidity. The humidity probably caused permanent changes to film. This might show up in new dimension measurement of the film but we were not able to do that.

The heatings did not effect much on conductivities. Due to contradictory results of heating measurements, too much conclusions should not be drawn from these values. After all the samples endured considerably well trough the measurements which gives some reference on the durability of the material too.

7 Conclusions

Thin films were prepared from DWCNT-xylan solution by drop casting and spinning. These films were imaged with optical microscope, AFM and TEM. Some roughness was noticed and on closer look the structure turned out to be random network of fibers. Significant amount of CNT ring structures were also found in the film.

Conductivity of the film was measured in room temperature and best sample achieved 1 600 S/cm conductivity which is very good from a CNT-cellulose film. This sample's conductivity improved even more during the measurements and peaked to 2 350 S/cm in heating experiments. The conductivity also seemed to remain well in lower temperatures until ~30 K. In 4.2 K temperature also non-ohmic behaviour was noticed which did not show in room temperature. Semiconductive properties were not seen in that temperature.

Theoretical models were applied on conductivity's dependency on temperature. FIT model worked well on temperature range of 7 – 32 K but VRH gave better fit on a bit higher temperatures of 30 – 180 K.

Effect of the environment was also tested in humidity and heating experiments. Humidities above 50 % RH seemed to drop the conductivity of the samples. When the humidity was lowered the conductivity return but the initial value was not achieved immediately. The humidity seemed to have bigger effect on thinner films. In heating experiments the samples were heated above 100 °C. We got mixed results from the effect of the heating but in conclusion could be said that the conductivity stays in 15 % tolerance on the tested higher temperature range.

References

[1] Zhuangchun Wu, Zhihong Chen, Xu Du, Jonathan M. Logan, Jennifer Sippel, Maria Nikolou, Katalin Kamaras, John R. Reynolds, David B. Tanner, Arthur F. Hebard, and Andrew G. Rinzler. Transparent, conductive carbon nanotube films. *Science*, 305(5688):1273–1276, 2004.

[2] Yeongun Ko, Nam Hee Kim, Na Rea Lee, and Suk Tai Chang. Meniscus-dragging deposition of single-walled carbon nanotubes for highly uniform, large-area, transparent conductors. *Carbon*, 77:964 – 972, 2014.

[3] Yangxin Zhou, Liangbing Hu, and George Grüner. A method of printing carbon nanotube thin films. *Applied Physics Letters*, 88(12), 2006.

[4] Hong-Zhang Geng, Ki Kang Kim, Kang Pyo So, Young Sil Lee, Youngkyu Chang, and Young Hee Lee. Effect of acid treatment on carbon nanotube-based flexible transparent conducting films. *Journal of the American Chemical Society*, 129(25):7758–7759, 2007. PMID: 17536805.

[5] Hua Xu, Steven M. Anlage, Liangbing Hu, and George Gruner. Microwave shielding of transparent and conducting single-walled carbon nanotube films. *Applied Physics Letters*, 90(18), 2007.

[6] Alexander Star, David W. Steuerman, James R. Heath, and J. Fraser Stoddart. Starched carbon nanotubes. *Angewandte Chemie International Edition*, 41(14):2508–2512, 2002.

[7] Oh-Kil Kim, Jongtae Je, Jeffrey W. Baldwin, Steven Kooi, Pehr E. Pehrsson, and Leonard J. Buckley. Solubilization of single-wall carbon nanotubes by supramolecular encapsulation of helical amylose. *Journal of the American Chemical Society*, 125(15):4426–4427, 2003. PMID: 12683805.

[8] Teruo Takahashi, Katsunori Tsunoda, Hirofumi Yajima, and Tadahiro Ishii. Dispersion and purification of single-wall carbon nanotubes

using carboxymethylcellulose. *Japanese Journal of Applied Physics*, 43(6R):3636, 2004.

[9] Online. `http://teachers.yale.edu/curriculum/extra/images/2010/10.05.02.01.jpg` Under public domain, updated 12.1.2015.

[10] Noriaki Hamada, Shin-ichi Sawada, and Atsushi Oshiyama. New one-dimensional conductors: Graphitic microtubules. *Physical Review Letters*, 68:1579–1581, Mar 1992.

[11] R. Saito, M. Fujita, G. Dresselhaus, and M. S Dresselhaus. Electronic structure of chiral graphene tubules. *Applied Physics Letters*, 60(18):2204–2206, 1992.

[12] Online. `http://upload.wikimedia.org/wikipedia/commons/thumb/3/35/CNTnames.png/300px-CNTnames.png` Under public domain, updated 12.1.2015.

[13] Veena Choudhary and Anju Gupta. *Carbon Nanotubes - Polymer Nanocomposites*, chapter Polymer/Nanocomposites. InTech, 2011.

[14] Nevill Francis Mott and Edward Davis. *Electronic Processes in Non-Crystalline Materials*. Oxford University Press, 2 edition, 1979.

[15] Ping Sheng. Fluctuation-induced tunneling conduction in disordered materials. *Physical Review B*, 21:2180–2195, Mar 1980.

[16] Hirotaka Koga, Tsuguyuki Saito, Takuya Kitaoka, Masaya Nogi, Katsuaki Suganuma, and Akira Isogai. Transparent, conductive, and printable composites consisting of tempo-oxidized nanocellulose and carbon nanotube. *Biomacromolecules*, 14(4):1160–1165, 2013.

[17] Naoki Imazu, Tsuyohiko Fujigaya, and Naotoshi Nakashima. Fabrication of flexible transparent conductive films from long double-walled carbon nanotubes. *Science and Technology of Advanced Materials*, 15(2):025005, 2014.

[18] Vincent C. Tung, Li-Min Chen, Matthew J. Allen, Jonathan K. Wassei, Kurt Nelson, Richard B. Kaner, and Yang Yang. Low-temperature solution processing of graphene – carbon nanotube hybrid materials for high-performance transparent conductors. *Nano Letters*, 9(5):1949–1955, 2009.

[19] Neerja Saran, Kunjal Parikh, Dong-Seok Suh, Edgar Muñoz, Harsha Kolla, and Sanjeev K. Manohar. Fabrication and characterization of thin films of single-walled carbon nanotube bundles on flexible plastic substrates. *Journal of the American Chemical Society*, 126(14):4462–4463, 2004.

[20] Seung Woo Lee, Byeong-Su Kim, Shuo Chen, Yang Shao-Horn, and Paula T. Hammond. Layer-by-layer assembly of all carbon nanotube ultrathin films for electrochemical applications. *Journal of the American Chemical Society*, 131(2):671–679, 2009.

[21] Nobutsugu Minami, Yeji Kim, Kanae Miyashita, Said Kazaoui, and Balakrishnan Nalini. Cellulose derivatives as excellent dispersants for single-wall carbon nanotubes as demonstrated by absorption and photoluminescence spectroscopy. *Applied Physics Letters*, 88(9), 2006.

[22] Robert C. Tenent, Teresa M. Barnes, Jeremy D. Bergeson, Andrew J. Ferguson, Bobby To, Lynn M. Gedvilas, Michael J. Heben, and Jeffrey L. Blackburn. Ultrasmooth, large-area, high-uniformity, conductive transparent single-walled-carbon-nanotube films for photovoltaics produced by ultrasonic spraying. *Advanced Materials*, 21(31):3210–3216, 2009.

[23] Liangbing Hu, Jang Wook Choi, Yuan Yang, Sangmoo Jeong, Fabio La Mantia, Li-Feng Cui, and Yi Cui. Highly conductive paper for energy-storage devices. *Proceedings of the National Academy of Sciences*, 106(51):21490–21494, 2009.

[24] N. P. Armitage, J.-C. P. Gabriel, and G. Güner. Quasi-langmuir–blodgett thin film deposition of carbon nanotubes. *Journal of Applied Physics*, 95(6):3228–3230, 2004.

[25] Yeji Kim, Nobutsugu Minami, Weihong Zhu, Said Kazaoui, Reiko Azumi, and Mutsuyoshi Matsumoto. Langmuir–blodgett films of single-wall carbon nanotubes:layer-by-layer deposition and in-plane orientation of tubes. *Jpn. J. Appl. Phys.*, 12(1):7629–7634, 2003.

[26] Jie Liu, Hongjie Dai, Jason H. Hafner, Daniel T. Colbert, Richard E. Smalley, Sander J. Tans, and Cees Dekker. Fullerene 'crop circles'. *Nature*, 385:780–781, 1997.

[27] Tobias Vossmeyer, Sung-Wook Chung, William M. Gelbart, and James R. Heath. Surprising superstructures: Rings. *Advanced Materials*, 10(4):351–353, 1998.

[28] M. Ahlskog, E. Seynaeve, R.J.M. Vullers, C. Van Haesendonck, A. Fonseca, K. Hernadi, and J. B.Nagy. Ring formations from catalytically synthesized carbon nanotubes. *Chemical Physics Letters*, 300(1–2):202–206, 1999.

[29] Richar Martel, Herbert R. Shea, and Phaedon Avouris. Rings of single-walled carbon nanotubes. *Nature*, 398:299, 1999.

[30] J.-F. Colomer, L. Henrard, E. Flahaut, G. Van Tendeloo, A. A. Lucas, and Ph. Lambin. Rings of double-walled carbon nanotube bundles. *Nano Letters*, 3(5):685–689, 2003.

[31] Xiao-Hua Zhong, Ya-Li Li, Feng Hou, and Jian-Min Feng. Formation and structure of circular-disc assemblies of double-walled carbon nanotubes from a catalytic cvd reaction. *Applied Physics A*, 92(3):709–713, 2008.

[32] M. F. Lin and D. S. Chuu. Persistent currents in toroidal carbon nanotubes. *Phys. Rev. B*, 57:6731–6737, Mar 1998.

[33] Lei Liu, G. Y. Guo, C. S. Jayanthi, and S. Y. Wu. Colossal paramagnetic moments in metallic carbon nanotori. *Phys. Rev. Lett.*, 88:217206, May 2002.

[34] H. R. Shea, R. Martel, and Ph. Avouris. Electrical transport in rings of single-wall nanotubes: One-dimensional localization. *Phys. Rev. Lett.*, 84:4441–4444, May 2000.

[35] Li Song, Lijie Ci, Chuanhong Jin, Pingheng Tan, Lianfeng Sun, Wenjun Ma, Lifeng Liu, Dongfang Liu, Zengxing Zhang, Yanjuan Xiang, Shudong Luo, Xiaowei Zhao, Jun Shen, Jianjun Zhou, Weiya Zhou, and Sishen Xie. Efficiently producing single-walled carbon nanotube rings and investigation of their field emission properties. *Nanotechnology*, 17(9):2355, 2006.

[36] Ning Li, Yi Huang, Feng Du, Xiaobo He, Xiao Lin, Hongjun Gao, Yanfeng Ma, Feifei Li, Yongsheng Chen, and Peter C. Eklund. Electromagnetic interference (emi) shielding of single-walled carbon nanotube epoxy composites. *Nano Letters*, 6(6):1141–1145, 2006.

[37] Bunshi Fugetsu, Eiichi Sano, Masaki Sunada, Yuzuru Sambongi, Takao Shibuya, Xiaoshui Wang, and Toshiaki Hiraki. Electrical conductivity and electromagnetic interference shielding efficiency of carbon nanotube/cellulose composite paper. *Carbon*, 46(9):1256–1258, 2008.

[38] Masanori Imai, Kousuke Akiyama, Tomo Tanaka, and Eiichi Sano. Highly strong and conductive carbon nanotube/cellulose composite paper. *Composites Science and Technology*, 70(10):1564–1570, 2010.

[39] Elena Bekyarova, Mikhail E. Itkis, Nelson Cabrera, Bin Zhao, Aiping Yu, Junbo Gao, and Robert C. Haddon. Electronic properties of single-walled carbon nanotube networks. *Journal of the American Chemical Society*, 127(16):5990–5995, 2005. PMID: 15839699.

[40] Hiromichi Ohta, Masahiro Orita, Masahiro Hirano, Hiroaki Tanji, Hiroshi Kawazoe, and Hideo Hosono. Highly electrically conductive indium-tin-oxide thin films epitaxially grown on yttria-stabilized

zirconia (100) by pulsed-laser deposition. *Applied Physics Letters*, 76(19):2740–2742, 2000.

[41] Sukang Bae, Hyeongkeun Kim, Youngbin Lee, Xiangfan Xu, Jae-Sung Park, Yi Zheng, Jayakumar Balakrishnan, Tian Lei, Hye Ri Kim, Young Il Song, Young-Jin Kim, Kwang S. Kim, Barbaros Ozyilmaz, Jong-Hyun Ahn, Byung Hee Hong, and Sumio Iijima. Roll-to-roll production of 30-inch graphene films for transparent electrodes. *Nature Nanotechnology*, 5(8):574–578, 2010.

[42] John E Fischer and Alan T Johnson. Electronic properties of carbon nanotubes. *Current Opinion in Solid State and Materials Science*, 4(1):28–33, 1999.

[43] Dongsheng Tang, Lijie Ci, Weiya Zhou, and Sishen Xie. Effect of h2o adsorption on the electrical transport properties of double-walled carbon nanotubes. *Carbon*, 44(11):2155–2159, 2006.

[44] Kaihui Liu, Wenlong Wang, Zhi Xu, Xuedong Bai, Enge Wang, Yagang Yao, Jin Zhang, and Zhongfan Liu. Chirality-dependent transport properties of double-walled nanotubes measured in situ on their field-effect transistors. *Journal of the American Chemical Society*, 131(1):62–63, 2009. PMID: 19093842.

[45] Alexander A. Green and Mark C. Hersam. Properties and application of double-walled carbon nanotubes sorted by outer-wall electronic type. *ACS Nano*, 5(2):1459–1467, 2011. PMID: 21280609.

[46] M Salvato, M Lucci, I Ottaviani, M Cirillo, S Orlanducci, E Tamburri, V Guglielmotti, F Toschi, M L Terranova, and M Pasquali. Low temperature conductivity of carbon nanotube aggregates. *Journal of Physics: Condensed Matter*, 23(47):475302, 2011.